Structure Formation under Steady-State Isothermal Planar Elongational Flow of *n*-Eicosane: A Comparison between Simulation and Experiment

T. C. Ionescu,[1] C. Baig,[1] B. J. Edwards,[1] D. J. Keffer,[1] and A. Habenschuss[2]

[1]*Department of Chemical Engineering, University of Tennessee, Knoxville, Tennessee 37996, USA*
[2]*Chemical Sciences Division, Oak Ridge National Laboratory, Oak Ridge, Tennessee 37831, USA*

(Received 11 October 2005; published 24 January 2006)

We use nonequilibrium molecular dynamics simulations to investigate the structural properties of an oriented melt of *n*-eicosane under steady-state planar elongational flow. The flow-induced structure was evaluated using the structure factor $s(k)$ taken as the Fourier transform of the total pair correlation function $g(r)$. We found that the equilibrium liquid structure factor is in excellent agreement with the one determined via x-ray diffraction. Moreover, a new x-ray diffraction experiment has been performed on a crystalline *n*-eicosane sample. The resulting intramolecular contribution to the structure factor was found to be in very good agreement with the simulated one at a high elongation rate, indicating the existence of a possible crystalline precursor structure.

DOI: 10.1103/PhysRevLett.96.037802 PACS numbers: 61.20.Ja, 36.20.Ey, 61.10.−i, 61.20.Gy

The crystallization of polymer melts under flow has generated a tremendous amount of interest over the years. Understanding crystallization mechanisms, kinetics, and crystallite morphologies are just a few of the problems that present an ongoing interest among research communities [1–3]. With the rapid advancements in computational capabilities and the development of new algorithms, molecular simulation techniques are playing an increasingly important role in elucidating these problems. Short and long chain *n*-alkanes have been extensively used to model the behavior of polyethylene, in particular, and polymers in general. In practice, polymers are known to form ordered domains when subjected to deformation either in the melt or solid states. In industrial applications such as fiber spinning or film blowing, this phenomenon is desired, and a precise control over the nucleation rates, crystallite growth, and morphology is critical. From an experimental perspective, it is very challenging to investigate the individual phenomena taking place during polymer crystallization, given the different length and time scales involved. This is why molecular simulation is potentially the ideal tool for investigating these processes.

Crystallization of long chain molecules from quiescent melts is particularly difficult to attain with the molecular simulation techniques available today, due to the long simulation times and atomistic-level detail needed to observe such phenomena. Extensive studies have been dedicated to characterizing melting and crystallization of *n*-alkanes under equilibrium conditions using molecular dynamics [4–11] or Monte Carlo [3,12,13] techniques. Even for the relatively short alkane chains, the simulation times needed to observe ordered phase formation are on the order of tens of nanoseconds, which is prohibitive on most supercomputers today. To this end, alternative methods have been proposed in order to enhance the crystallization rates, which include crystallization in the presence of a surface [2] or increasing the melting point by driving the system away from equilibrium via uniaxial stretching [7,14,15] or shear flow [6,16,17].

In rheology, there are two major types of flow: elongational flow and shear flow. For shear flow, there have been many successful attempts at developing nonequilibrium molecular dynamics (NEMD) algorithms for simulating rheological and structural properties of chain molecules. Phenomena such as shear thickening, associated with crystalline structure formation under extreme shear rates, have also been reported [6,17]. In the past several years, NEMD algorithms have also been developed for simulating the rheological and structural properties of liquids under planar elongational flow (PEF).

Some recent studies focused on characterizing the crystallization behavior of oriented *n*-alkane melts [7,14,15] by means of uniaxial stretching. It should be noted, however, that no rigorous NEMD algorithm capable of steady-state simulation was employed in any of these studies. The uniaxial stretching was accomplished by applying an artificial stress in one preferred direction for a short period of time (usually on the order of 1 ns). By doing this, the Newtonian dynamics were altered and any physical quantity measured during this time frame would be subject to doubt. That is probably the reason why the authors only applied this stretching technique in order to obtain ''stretched amorphous configurations,'' and all meaningful physical quantities were measured after the applied stress was turned off. While providing valuable insight upon crystallization mechanisms and kinetics at various temperatures and for various chain lengths after the applied stress stopped, these methods are equilibrium MD simulations using stretched initial configurations.

In the present study, we have employed a proper NEMD algorithm, and the transition to the crystallinelike structure was observed during steady-state PEF; therefore, the present case is much more relevant to a real physical

situation of flow-induced crystallization at a constant temperature above the melting point.

Aspects concerning the simulation method and algorithm, as well as the potential model used to describe the interactions between the atomistic chains, have been presented in detail in two previous papers [18–20], and will not be presented here. In the present study we focus our attention on the structural properties of eicosane, and comparison with experimental x-ray diffraction data for both the liquid and crystalline states.

In a typical x-ray diffraction experiment, the quantity measured is the static structure factor, $s(k)$. The structure factor is of particular importance to molecular simulation, because its Fourier transform gives the total pair correlation function, $g(r)$, through the equation

$$g(r) = 1 + (2\pi^2 r\rho_0)^{-1} \int_0^\infty k(s(k) - 1)\sin(kr)dk, \quad (1)$$

where k is the wave number and ρ_0 is the particle number density.

The total pair correlation function, $g(r)$, is a quantity readily available from any molecular level simulation, and, conversely, it can be transformed to obtain the static structure factor through the equation

$$s(k) = 1 + \frac{4\pi\rho_0}{k} \int_0^\infty r(g(r) - 1)\sin(kr)dr. \quad (2)$$

Thus, Eqs. (1) and (2) allow us to compare directly structural information obtained from simulation and x-ray diffraction experiments.

First, let us examine the liquid structure of n-eicosane predicted by simulation under equilibrium conditions. In Fig. 1, the simulated static structure factor computed as the Fourier transform of the total pair correlation function, $g(r)$, [Eq. (2)] is shown. We make a distinction here between the total pair correlation function $g(r)$ [Fig. 2(a)], and the intermolecular pair correlation function $g\_\text{inter}(r)$ [Fig. 2(b)]. For $g(r)$, the distance distribution is computed between pairs involving all sites (CH_2 groups) in the system, while for $g\_\text{inter}(r)$, distances between pairs of sites belonging to the same chain were excluded. Consequently, there are two structure factors associated with each pair correlation function, the total structure factor, $s(k)$ [Fig. 2(c)], and the intermolecular structure factor, $s\_\text{inter}(k)$ [Fig. 2(d)].

The liquid n-eicosane was simulated in the NVT ensemble, where the total number of particles N, the simulation box volume V, and the temperature T, are kept constant. In Fig. 1, comparison is made with existing x-

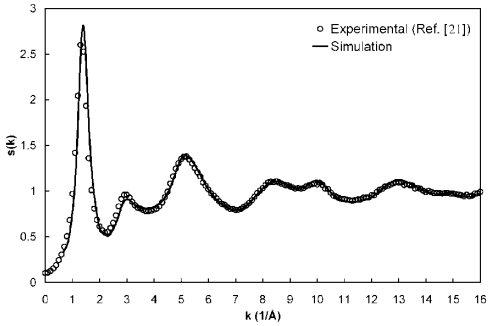

FIG. 1. Comparison of the structure factor, $s(k)$, between experiment (Ref. [21]), and simulation under quiescent conditions at $T = 315$ K and $\rho = 0.81$ g/cm^3.

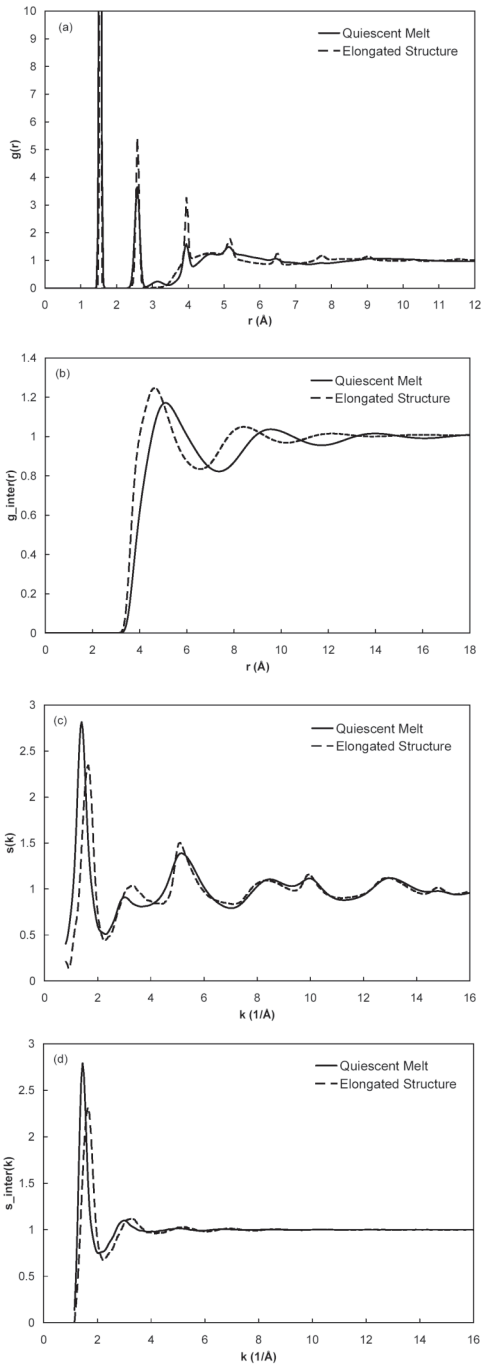

FIG. 2. Simulated structures in terms of: (a) total pair correlation function $g(r)$; (b) intermolecular pair correlation function $g\_\text{inter}(r)$; (c) total static structure factor $s(k)$; (d) intermolecular static structure factor $s\_\text{inter}(k)$ at $T = 315$ K and $\rho = 0.81$ g/cm^3.

ray scattering data for liquid *n*-eicosane [21]. The simulation was performed employing 200 eicosane molecules in the cubic box with each side of 48.7 Å at the same state point as the experiment ($T = 315$ K and $\rho = 0.81$ g/cm^3). As clearly shown in Fig. 1, we see an excellent agreement between the simulated and experimentally determined liquid structures.

Let us now examine the structure when the flow field is turned on at steady state, at a reduced elongation rate $\dot{\varepsilon}(m\sigma^2/\varepsilon)^{1/2} = 1.0$. Here, $\dot{\varepsilon}$ denotes the elongation rate, m mass of the CH_2 group, and σ and ε, respectively, the size and energy parameters of the CH_2 group in the Lennard-Jones potential. It is worth pointing out that the temperature and density were maintained constant throughout the flow simulation at $T = 315$ K and $\rho = 0.81$ g/cm^3, respectively; thus any differences we see are due neither to temperature nor density changes, but to structural rearrangements. For the NEMD simulation, we employed 648 eicosane molecules using a noncubic box, since x and y dimensions are contracting and extending with time (after applying the initial orientation angle), and chains are aligned and extended in those directions. The box dimension ($x \times y \times z$ in unit of Å) of $90.4 \times 90.4 \times 47.2$ was chosen, in particular, for x and y dimensions, to be much larger than the fully stretched chain length with the *trans* conformation of 24.5 Å for $C_{20}H_{42}$ in order to eliminate any system-size effect.

In Figs. 2(a) and 2(b), we present the total and intermolecular pair correlation functions $g(r)$ and $g\_\text{inter}(r)$ respectively, under quiescent and steady-state flow conditions. In Fig. 2(a), it is readily observed that the peak at 3.16 Å in the total pair correlation function for the quiescent melt has completely vanished in the elongated structure. This peak is associated with the 1–4 pair distance on the same chain in the *gauche* conformation, and its disappearance is indicative that the chains have adopted the all-*trans* fully extended conformation. This fact is also supported by the heightening of the peak at 3.94 Å, which is associated with the 1–4 pair distance on the same chain in the *trans* conformation. On the same note, the 1–2 and 1–3 peaks at 1.54 and 2.58 Å, respectively, also present significant narrowing and increase in height. This is a clear indication that the distribution around the respective equilibrium distances is narrowed in the elongated state. These facts represent the first indication of a transition to a crystallinelike precursor state where the individual molecular chains take on conformations very similar to those in the solid phase. Moreover, the narrowing of the peaks is indicative of a freezing out of the low wavelength vibrational degrees of freedom, another shift toward a solid phase. Evidence in the form of the decrease in the vibrational energy as a function of elongation rate for decane, hexadecane, and tertacosane corroborates this statement [19]. In Fig. 2(b), one notices that all intermolecular peaks have shifted towards lower distances and heightened in the elongated state compared to the quiescent melt. This is very important, and is indicative of closer lateral packing distances between neighboring chains. As a reminder, both pair correlation functions in Fig. 2(b) were generated under the same temperature and density conditions, thus the differences arise solely from structural rearrangements.

Mirroring the pair correlation functions [Figs. 2(a) and 2(b)], we focus our attention now on the total and intermolecular static structure factors [Figs. 2(c) and 2(d), respectively]. We readily observe the shift of the first peak at $k = 1.4$ in the equilibrium melt structure towards a higher value ($k = 1.65$) in the elongated state. As Fig. 2(d) clearly shows, this peak is solely associated with intermolecular distances, and the shift mirrors the shift in the first peak in Fig. 2(b).

With the view of comparing the simulated structure factor for the elongated structures to the measured one for the crystal, we undertook x-ray scattering measurements from *n*-eicosane in the solid state. The *n*-eicosane, $C_{20}H_{42}$, was measured at room temperature (melting point 36–38 °C), and the x-ray measurements were in reflection geometry using MoK_α radiation ($\lambda = 0.71\,069$ Å). The range of scattering angles covered the interval $0.16 < k < 16$ Å^{-1}, where $k = (4\pi/\lambda \sin\theta)$, with 2θ the scattering angle. Corrections for background, absorption, polarization, incoherent scattering, detector energy discrimination, and multiple scattering were applied.

Following the procedure for the analysis of the *n*-eicosane melt [21], the corrected, measured scattering pattern of the crystalline material was normalized to the scattering expected from uncorrelated, independent scattering sites CH_3 and CH_2. We use ''united atom'' scattering factors for CH_3 and CH_2 [22], since the simulations were performed using united atom sites.

The structure factor, $s(k)$, for the crystalline material is compared to the melt in Fig. 3(a). The sharp Bragg peaks below $k = 6$ Å^{-1} have been indexed in a triclinic unit cell, and the unit cell parameters obtained by least-squares refinement of 22 reflections are $a = 4.322(9)$ Å, $b = 4.799(10$ Å), $c = 27.43(5)$ Å, $\alpha = 84.98(35)°$, $\beta = 67.48(23°)$, $\gamma = 72.03(28°)$, and $V = 499.6$ Å^3. These are in good agreement with literature values [23].

The dominant contributions to the structure factors at large $k(> \sim 6$ Å$^{-1})$, for both the melt and the crystalline material, are from the local intramolecular structure. These intramolecular contributions consist of correlations between sites within the molecular chain; that is, from bonded carbon atoms, C1-C2, C1-(C2)-C3, C1-(C2-C3)-C4, etc., These correlations determine the short-range order of the molecular chains, in that correlations C1-C4 and higher depend on the internal rotations along the carbon chain. The C1-C2 distance is simply the carbon-carbon bond distance in the chain; the C1-C3 distance is determined by the C1-C2 bond distance and the C1-C2-C3 bond angle; for the C1-C4 correlation distances we can have values that correspond to *trans* (*t*) and *gauche* (*g*) confor-

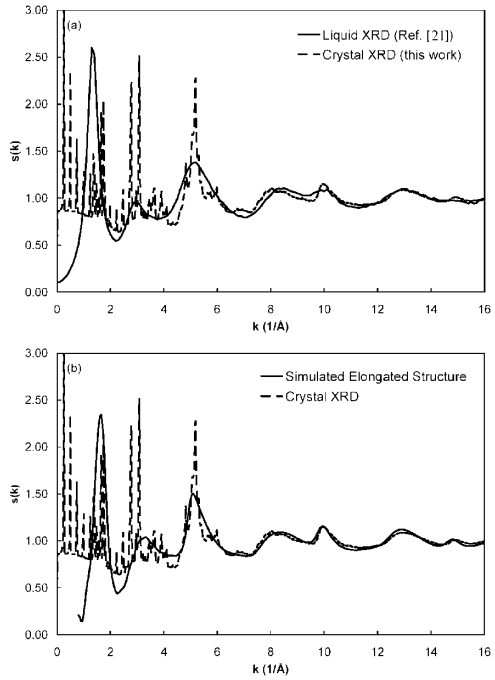

FIG. 3. (a) Structure comparison in terms of x-ray diffraction data between liquid (Ref. [21]) and crystalline *n*-eicosane; (b) Structure comparison in terms of total static structure factor between x-ray diffraction data for the crystalline *n*-eicosane and the simulated elongated structure.

mations; for the C1-C5 correlations we can have distances corresponding to *tt*, *tg*, and *gg* conformations, and so on. Clearly, for the *n*-eicosane melt, we should have an equilibrium between the *trans* and *gauche* conformations determined by the rotational potential of the C-C bond. In the case of the crystalline material, the molecular chains are forced into an all-*trans* conformation dictated by the crystal structure. So these differences in the melt and crystalline intramolecular structure will appear in the high-k region of the structure factor. Beyond the Bragg peaks, the structure factors for the melt and the crystalline material in Fig. 3(a) differ significantly. The crystal structure factor shows sharper features at 5, 10, and 15 Å^{-1}, and overall, all the peaks are asymmetric compared to the melt. This is also in quantitative agreement with simulation, as it is readily observable in Figs. 2(c) and 3(b).

To conclude, the local intramolecular structure has been found to be in very good quantitative agreement with the actual crystalline structure of *n*-eicosane. The molecules adopt the all-*trans* fully stretched conformations, with closer lateral chain packing distances. However, we found no evidence of global long-range order, which would qualify the elongated structures as truly crystalline. However, the excellent agreement between simulation and experiment for $k > 5$ Å^{-1} suggests that the individual chains have taken on conformations consistent with a precursor structure to the crystalline phase. The lack of global long-range order might be due to the simulation technique, where the structure has not been allowed to relax under a constant pressure algorithm; i.e., the volume change between the liquid and solid phases has not been allowed. Moreover, the applied planar elongational deformation rate might also be too low for the long-range order to form; i.e., the simulation is limited at high elongational rates by thermostat artifacts.

This research was supported by the donors of the Petroleum Research Fund, administered under Grant No. 41000-AC7. This research project also used resources of the Center for Computational Sciences and the x-ray facilities at the Oak Ridge National Laboratory, which is supported by the Office of Science, U.S. Department of Energy, under Contract No. DE-AC05-00OR22725 with Oak Ridge National Laboratory, managed and operated by UT-Battelle, LLC.

[1] C. Liu and M. Muthukumar, J. Chem. Phys. **109**, 2536 (1998).
[2] N. Waheed, M. S. Lavine, and G. C. Rutledge, J. Chem. Phys. **116**, 2301 (2002).
[3] D. M. Sadler, and G. H. Gilmer, Phys. Rev. Lett. **56**, 2708 (1986).
[4] H. Meyer and F. Muller-Plathe, Macromolecules **35**, 1241 (2002).
[5] K. Esselink, P. A. J. Hilbers, and B. W. H. Vanbeest, J. Chem. Phys. **101**, 9033 (1994).
[6] R. A. Gray, P. B. Warren, S. Chynoweth, Y. Michopoulos, and G. S. Pawley, Proc. R. Soc. A **448**, 113 (1995).
[7] A. Koyama *et al.*, J. Macromol. Sci., Phys. **B42**, 821 (2003).
[8] S. Fujiwara and T. Sato, J. Chem. Phys. **110**, 9757 (1999).
[9] Q. Liao and X. G. Jin, J. Chem. Phys. **110**, 8835 (1999).
[10] T. A. Kavassalis and P. R. Sundararajan, Macromolecules **26**, 4144 (1993).
[11] H. Takeuchi, J. Chem. Phys. **109**, 5614 (1998).
[12] L. Toma, S. Toma, and J. A. Subirana, Macromolecules **31**, 2328 (1998).
[13] G. Q. Xu, H. Lin, and W. L. Mattice, J. Chem. Phys. **119**, 6736 (2003).
[14] M. J. Ko, N. Waheed, M. S. Lavine, and G. C. Rutledge, J. Chem. Phys. **121**, 2823 (2004).
[15] M. S. Lavine, N. Waheed, and G. C. Rutledge, Polymer **44**, 1771 (2003).
[16] P. J. Daivis, D. J. Evans, and G. P. Morriss, J. Chem. Phys. **97**, 616 (1992).
[17] G. P. Morriss, P. J. Daivis, and D. J. Evans, J. Chem. Phys. **94**, 7420 (1991).
[18] C. Baig, B. J. Edwards, D. J. Keffer, and H. D. Cochran, J. Chem. Phys. **122**, 114103 (2005).
[19] C. Baig, B. J. Edwards, D. J. Keffer, and H. D. Cochran, J. Chem. Phys. **122**, 184906 (2005).
[20] B. J. Edwards, C. Baig, and D. J. Keffer, J. Chem. Phys. **123**, 114106 (2005).
[21] A. Habenschuss and A. H. Narten, J. Chem. Phys. **92**, 5692 (1990).
[22] A. H. Narten, J. Chem. Phys. **70**, 299 (1979).
[23] S. C. Nyburg and A. R. Gerson, Acta Crystallogr. Sect. B **48**, 103 (1992).